Geophysical Research Letters

RESEARCH LETTER
10.1029/2024GL111046

Electrical Conductivity of (Mg, Fe)CO_3 at the Spin Crossover and Its Implication for Mid-Mantle Geomagnetic Heterogeneities

Chaoshuai Zhao[1], Jin Liu[2], Liangxu Xu[3], Mingqiang Hou[4], Yukai Zhuang[5], Jie Zhu[6], and Jung-Fu Lin[7]

[1]Deep Space Exploration Laboratory/School of Earth and Space Sciences, University of Science and Technology of China, Hefei, China, [2]Center for High Pressure Science, State Key Laboratory of Metastable Materials Science and Technology, Yanshan University, Qinhuangdao, China, [3]School of Earth and Space Sciences, Peking University, Beijing, China, [4]State Key Laboratory of Geodesy and Earth's Dynamics, Innovation Academy for Precision Measurement Science and Technology, Chinese Academy of Sciences, Wuhan, China, [5]Institute of Atomic and Molecular Physics, Sichuan University, Chengdu, China, [6]College of Science, Guizhou Institute of Technology, Guiyang, China, [7]Jackson School of Geosciences, The University of Texas at Austin, Austin, TX, USA

Abstract (Mg, Fe)CO_3 is an important deep carbon carrier and plays a vital role in our understanding of lower-mantle carbon reservoirs. The electrical conductivity (EC) of $FeCO_3$ was measured at 126−2000 K up to 83 GPa in diamond-anvil cells using a standard four-probe van der Pauw method. Moreover, the EC of $FeCO_3$ increases by ∼6 orders of magnitude from 300 to 1500 K at 10−20 GPa, indicating a strong effect of high temperature. The EC of $Fe_{0.65}Mg_{0.35}CO_3$ was measured up to 60 GPa at 300 K, the EC values of (Mg, Fe)CO_3 are proportional to iron content and increase by 2–3 orders of magnitude at 300 K across the spin crossover. The EC values of (Mg, Fe)CO_3 and $FeCO_3 + Fe_3O_4 \pm C$ mixtures surpass that of bridgmanite, ferropericlase and davemaoite by ∼1–4 orders of magnitude at depths of 800–2,000 km. This result sheds insights into the genesis of local geomagnetic heterogeneities in the mid-lower mantle.

Plain Language Summary Geomagnetic observations reveal electrical heterogeneities in the mid-lower mantle. However, some of the aforementioned geomagnetic anomalies are higher than the electrical conductivity (EC) values of major lower-mantle minerals such as ferropericlase, bridgmanite, and davemaoite. This calls for the existence of high conductive mineral(s) in the region where subducting slabs can bring certain amounts of Fe-bearing and/or carbon-bearing materials. In this study, we report that EC values of (Mg, Fe)CO_3 and $FeCO_3 + Fe_3O_4 \pm C$ mixtures are 1–4 orders of magnitude greater than that of the major minerals at depths of 800–2,000 km. This suggests (Mg, Fe)CO_3-bearing and its decomposed mixtures subducting patches may induce local geomagnetic heterogeneities at these depths. In particular, these materials may contribute to the geomagnetic anomalies observed at ∼1,300 km depths and assist in identifying potential carbon-rich regions in the lower mantle.

Key Points:

- Electrical conductivity (EC) of $FeCO_3$ was measured at 126−2000 K and 0–83 GPa using the van der Pauw method in diamond-anvil cells
- EC of (Mg, Fe)CO_3 is proportional to iron content and increases by 2–3 orders of magnitude at the spin crossover
- High conductivity of (Mg, Fe)CO_3 and $FeCO_3 + Fe_3O_4 \pm C$ mixtures may contribute to local geomagnetic heterogeneities in the mid-lower mantle

Supporting Information:

Supporting Information may be found in the online version of this article.

Correspondence to:

J. Zhu and J. Liu,
jiezh_16@163.com;
jinliu@ysu.edu.cn

Citation:

Zhao, C., Liu, J., Xu, L., Hou, M., Zhuang, Y., Zhu, J., & Lin, J.-F. (2024). Electrical conductivity of (Mg, Fe)CO_3 at the spin crossover and its implication for mid-mantle geomagnetic heterogeneities. *Geophysical Research Letters*, *51*, e2024GL111046. https://doi.org/10.1029/2024GL111046

Received 26 JUN 2024
Accepted 29 OCT 2024

Author Contributions:

Conceptualization: Chaoshuai Zhao, Jin Liu, Jung-Fu Lin
Data curation: Chaoshuai Zhao, Liangxu Xu, Mingqiang Hou, Yukai Zhuang, Jie Zhu
Formal analysis: Chaoshuai Zhao, Jie Zhu
Funding acquisition: Chaoshuai Zhao, Jin Liu, Mingqiang Hou
Investigation: Chaoshuai Zhao, Jin Liu
Methodology: Chaoshuai Zhao, Jin Liu, Liangxu Xu, Mingqiang Hou, Yukai Zhuang, Jie Zhu, Jung-Fu Lin
Project administration: Jin Liu
Resources: Jin Liu, Jie Zhu, Jung-Fu Lin

1. Introduction

Deep carbon cycle significantly influences the climate and habitability evolution of Earth's surface, and the exchange efficiency between the surface and the deep mantle (Behn et al., 2011; Foley & Fischer, 2017; Kelemen & Manning, 2015; Lee et al., 2016; Plank & Manning, 2019; Poli, 2015; Thomson et al., 2016). Carbon, with its relatively low solubility in the silicate mantle, primarily exists as accessory minerals such as carbonates, diamond, graphite, and carbides in the Earth's interior (Hazen & Schiffries, 2013; Shcheka et al., 2006). It is estimated that about 82 ± 14 Mt of carbon is recycled into the Earth's interior via subduction slabs each year (Plank & Manning, 2019). Petrologic and geochemical signatures evidence that carbon is mainly subducted in the form of carbonates (e.g., Plank & Manning, 2019; Sanchez-Valle et al., 2011). Together with Zn isotopic compositions in the deep-mantle materials, the coexistence of carbonates and davemaoite ($CaSiO_3$-perovskite) in superdeep diamond inclusions further supports the presence of carbonates in the Earth's deep mantle (Brenker et al., 2007; Maeda et al., 2017; Zhang et al., 2022). Previous studies have shown that carbonates can affect the physical and chemical properties of the Earth's mantle, including elasticity, electrical conductivity (EC), thermal conductivity, viscosity, and melting curve through carbon-induced partial melting (Chao & Hsieh, 2019; Fu et al., 2017; Gaillard et al., 2008; Liu et al., 2014; Marcondes et al., 2016; Sun et al., 2020; Thomson et al., 2016). Understanding the

Supervision: Jin Liu
Validation: Chaoshuai Zhao
Writing – original draft: Chaoshuai Zhao, Jin Liu
Writing – review & editing: Chaoshuai Zhao, Jin Liu, Liangxu Xu, Mingqiang Hou, Yukai Zhuang, Jie Zhu, Jung-Fu Lin

physical and chemical properties of carbonate minerals under deep mantle conditions is crucial for constraining the deep carbon cycle, as well as the chemistry and dynamics of various geological processes (e.g., metamorphism and earthquake) (Fu et al., 2017; Isshiki et al., 2004; Prakash et al., 2023; Sun et al., 2020; Thomson et al., 2016; Zhao, Mao, et al., 2024).

(Mg, Fe)CO_3 solid solutions have been recognized as major carbon carriers in the deep mantle (Cerantola et al., 2017; Farsang et al., 2021; Isshiki et al., 2004; Liu et al., 2015; Lv et al., 2021; Pan et al., 2013). Similar to major iron-bearing mantle minerals, ferropericlase (Mg, Fe)O and bridgmanite (Mg, Fe) (Al, Si)O_3 in the lower mantle, (Mg, Fe)CO_3 solid solutions display abnormal elasticity, sound velocity, compressibility, thermal and EC properties across the electronic spin-pairing transition of iron at high pressure-temperature (*P-T*) conditions (Cerantola et al., 2015; Chao & Hsieh, 2019; Fu et al., 2017; Lin et al., 2013; Liu et al., 2014; Z. Mao et al., 2011, 2015). Notably, the electronic spin transition of iron decreases the EC of ferropericlase and bridgmanite under mantle pressures (Lin et al., 2007; Liu et al., 2018; Ohta et al., 2007, 2010; Yoshino et al., 2011), which cannot contribute to the local geomagnetic anomalies with a jump of ∼1.2 $\log_{10}$S/m at ∼1,300 km depths according to magnetotelluric data and geomagnetic depth sounding observations (Constable & Constable, 2004; Kuvshinov et al., 2005; Kuvshinov & Olsen, 2006; Velímský, 2010). Particularly, the electrical anomalies at ∼1,300 km coincide within the spin crossover of (Mg, Fe)CO_3 at deep mantle *P-T* conditions (Cerantola et al., 2017; Liu et al., 2014). Moreover, (Mg, Fe)CO_3 solid solutions exhibit abnormal thermal conductivity properties across the spin crossover (Chao & Hsieh, 2019). Given the connection between thermal and EC, knowledge of the electrical behavior of (Mg, Fe)CO_3 at lower-mantle conditions is therefore necessary to help decode the geomagnetic anomalies at mid-mantle depths.

Thus far, EC measurements on (Mg, Fe)CO_3 solid solutions have been limited to $MgCO_3$ and $FeCO_3$ end-members at relatively moderate pressure and temperature conditions (H. Hu et al., 2022; Mibe & Ono, 2011; Papathanassiou, 1998). The EC of $MgCO_3$ was measured up to 0.3 GPa at 300 K using a piston-cylinder apparatus (Papathanassiou, 1998), and the investigated *P-T* conditions were elevated to 6 GPa and 1000 K using a multi-anvil apparatus (Mibe & Ono, 2011). Recently, iron-rich $(Fe_{0.88}Mg_{0.09}Mn_{0.03})CO_3$ was measured up to 3 GPa and 973 K (H. Hu et al., 2022). To date, however, little is known about the EC properties of (Mg, Fe)CO_3 at high *P-T* conditions relevant to the lower mantle, especially across the spin transition of iron. Therefore, it is crucial to clarify the EC of (Mg, Fe)CO_3 across the spin crossover under lower-mantle conditions. Considering the strongly negative values of iron partitioning coefficient for $FeCO_3$ with respect to bridgmanite, and the low-spin iron ion being energetically more stable at high pressures than its high-spin counterpart, it is conceivable that the composition of carbonates in the Earth's lower mantle could thus be significantly enriched toward the "$FeCO_3$" component (Cerantola et al., 2017; Dasgupta et al., 2004; J. Hu et al., 2023; Lin et al., 2013; Liu et al., 2015; Timmerman et al., 2021).

In the present work, we conducted EC measurements on the two representative iron-rich (Mg, Fe)CO_3 samples with minor amounts of Mn at 126−2000 K and pressures up to 83 GPa using the standard four-probe van der Pauw method in diamond anvil cells (DACs). It was observed that EC values of (Mg, Fe)CO_3 are proportional to iron content, experiencing a dramatic increase by 2–3 orders of magnitude at the spin crossover. Furthermore, the EC values of (Mg, Fe)CO_3 increase significantly by ∼6–8 orders of magnitude with increasing temperature from 300 to 1500 K. These findings provide insights into the effects of high pressure, high temperature, and iron content on the EC evolution of (Mg, Fe)CO_3 solid solutions. These results are used to understand anomalous EC profiles in the mid-lower mantle where subducting slabs can accumulate Fe-bearing and/or carbon-bearing materials.

2. Experimental Methods

2.1. Sample Characterization

Two (Mg, Fe)CO_3 samples were used in this study. Naturally occurring siderite (no. NMNH R11313) from the Tsumeb Mine (Namibia) was obtained from the Department of Mineral Sciences, Smithsonian Institution. Composition analysis using an electron microscope (JEOL JXA-8200) confirms the chemical composition of $FeCO_3$, with minor $MnCO_3$ (<0.2 mol%). It is referred to as $FeCO_3$ hereafter. The other (Mg, Fe)CO_3 sample with a chemical composition of $(Fe_{0.65}Mg_{0.33}Mn_{0.02})CO_3$, denoted as $(Fe_{0.65}Mg_{0.35})CO_3$ for simplicity, was used to further evaluate the compositional effect on EC. The characterizations of both samples have already been reported by Liu et al. (2015).

2.2. High-Pressure Electrical Measurements

Rhenium gaskets were pre-indented to approximately 25 μm in thickness. A hole of 180 or 280 μm in diameter was then drilled at the center of the pre-indention. Cubic boron nitride (c-BN) fine powders were packed into the hole, electrically insulating the metal gasket from the sample and electrodes. Another hole of 70 μm in diameter was drilled at the center of the c-BN gasket insert as a sample chamber. This chamber was filled with soft hexagonal boron nitride (h-BN) or sodium chloride (NaCl) fine powders to serve as a pressure-transmitting medium and an insulation layer between the diamond anvil culet and the carbonate sample. Polycrystalline $FeCO_3$ and $(Fe_{0.65}Mg_{0.35})CO_3$ samples were gently pressed to form a disk of ∼5 μm thick and ∼40 μm in diameter and then loaded into the sample chamber, respectively. The sample disk was connected with sharp gold electrodes in the van der Pauw configuration using the standard four-probe direct current techniques. Whole electrical resistance was in-situ measured using a Keithley 6517A electrometer in direct current. Although the measured resistance is fairly accurate, the uncertainty of obtained EC values may be up to 30% (Lin et al., 2007).

High pressure was generated using a pair of diamond anvils with a culet size of 200 or 300 μm. The pressure at 126−300 K was determined by the ruby fluorescence scale, and its uncertainty was calculated from multiple measurements on the three small ruby spheres (H. Mao et al., 1986). For low-temperature experiments, the DAC was gradually cooled down to 126 K using liquid nitrogen, and temperatures were obtained from a K-type thermocouple attached to the diamond anvil table. For high pressure and temperature experiments, the pressure was calibrated based on the Raman spectra of the diamond culet atop the sample (Akahama & Kawamura, 2010). High temperature was generated using the laser heating system at the Center for High Pressure Science and Technology Advanced Research. The system was equipped with a ytterbium CW fiber laser with a wavelength of 1,070 nm and the laser spot on the sample position was ∼30 μm in full width at half maximum (Hou et al., 2021). Thermal radiation spectra of the heated sample were fitted to the Planck radiation function assuming the graybody approximation and the temperature uncertainty was about ±150 K from both sides of the sample (Shen et al., 2001). The $FeCO_3$ sample was heated by laser heating and maintained for at least 10 min before the in-situ EC measurement at simultaneous high *P-T*.

3. Results and Discussion

3.1. High-Pressure EC of (Mg, Fe)CO_3 Across the Spin Transition of Iron

The EC of $FeCO_3$ was measured at low temperatures, down to 185 K at 21 GPa and 126 K at 62 GPa, respectively, to clarify the conduction mechanism of (Mg, Fe)CO_3 below pre-melting temperature (Figure S1 and Text S1 in Supporting Information S1 for more details). The measured EC values from 126 to 300 K were fitted to the Arrhenius equation to derive the activation energy and activation volume. The derived activation energy and activation volume are 0.227 eV and −0.048 cm^3/mol, respectively, at 21 GPa. They decrease to 0.157 eV and −0.054 cm^3/mol at 62 GPa, consistent with the small polaron conduction (electronic hopping in Fe^{2+}-Fe^{3+}) (Yoshino, 2010). The conduction mechanism derived in this DAC study agrees well with the previous EC work on $MgCO_3$ and $(Fe_{0.88}Mg_{0.09}Mn_{0.03})CO_3$ at 1−6 GPa and 373−1000 K using a multi-anvil apparatus (H. Hu et al., 2022; Mibe & Ono, 2011). The small polaron conduction mechanism remains dominant in the EC of $FeCO_3$ at elevated temperatures, as do the major lower-mantle minerals of bridgmanite and ferropericlase (Dobson & Brodholt, 2000; Yoshino, 2010; Yoshino et al., 2016).

Further, the EC values of $FeCO_3$ were measured up to 83 GPa at room temperature (Figure 1). Two independent runs were conducted for $FeCO_3$ at high pressure and room temperature using different DACs. The results are in excellent agreement with each other. Between 1 bar and 10 GPa, the EC of $FeCO_3$ increases by approximately one order of magnitude due to sample compaction and rapid change in grain boundaries upon initial compression in DACs. The EC values of $FeCO_3$ show a slight increase from 10 to 38 GPa in the high-spin state (Figure 1), indicating marginal changes in charge carrier density and mobility. Notably, the EC values of $FeCO_3$ exhibit a dramatic rise at pressures ranging from approximately 38 to 52 GPa, aligning with the pressure range for the electronic spin-pairing transition of iron in $FeCO_3$, as detected by X-ray diffraction and Raman spectroscopic studies (Zhao et al., 2020). The pressure dependence of $FeCO_3$ conductivity [$d(\log_{10}S/m)/dP$] throughout the spin crossover is nearly ∼14 times greater than that in the high-spin state at 10−38 GPa. This substantial increase in the EC is attributed to the iso-symmetric high-spin to low-spin transition of iron in $FeCO_3$, accompanied by a large volume collapse (Lavina et al., 2009, 2010; Liu et al., 2015; Mattila et al., 2007). The pressure-induced electronic spin transition of iron significantly alters the mobility and density of charge carriers in the mixture

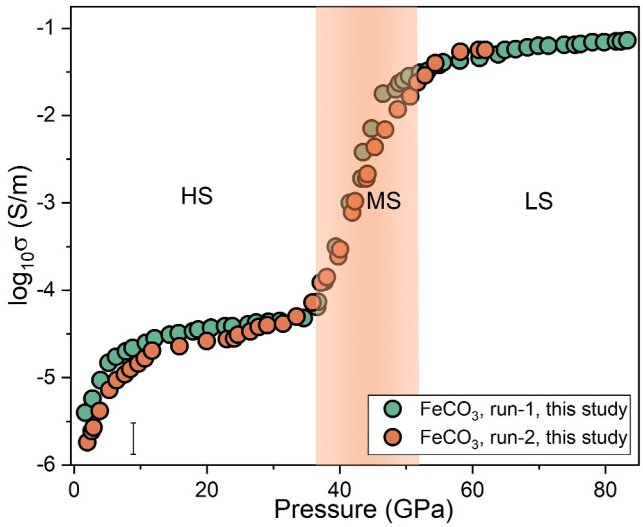

Figure 1. Electrical conductivity (EC) of $FeCO_3$ as a function of pressure at 300 K. Green and orange circles represent the first and second runs of EC experiments for $FeCO_3$, respectively. The orange region is the spin crossover of $FeCO_3$ at 300 K. The EC of $FeCO_3$ increases dramatically at the spin crossover. HS, MS, and LS represent the high-spin, mixture spin (i.e., high-spin + low-spin), and low-spin states, respectively. The error bar is shown as a vertical tick on the left bottom for clarity.

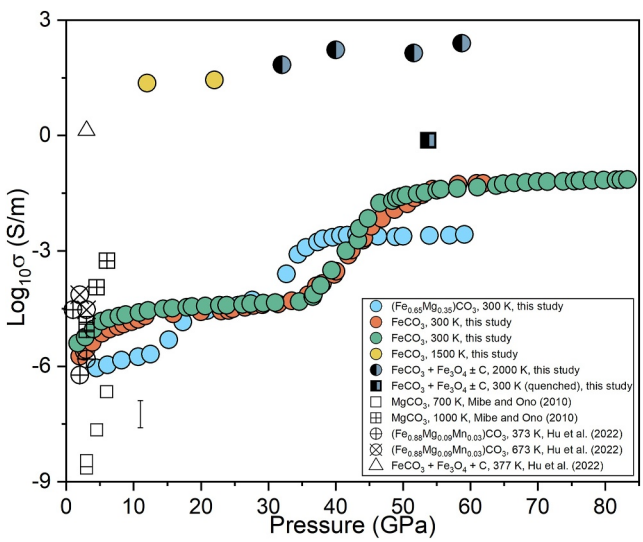

Figure 2. Electrical conductivity of (Mg, Fe)CO_3 at varying temperatures with increasing pressure. Green and orange solid circles: $FeCO_3$ at 300 K, this study; yellow solid circles: $FeCO_3$ at 1500 K, this study; half-filled circles: the mixture of $FeCO_3 + Fe_3O_4 \pm C$ at 2000 K, this study; half-filled square: the mixture of $FeCO_3 + Fe_3O_4 \pm C$ quenched from 58 GPa to 2000 K, this study; blue solid circles: $Fe_{0.65}Mg_{0.35}CO_3$ at 300 K, this study. Black open triangles: the quenched mixture $FeCO_3 + Fe_3O_4 + C$ at 3 GPa and 373 K, by H. Hu et al. (2022); open circles with crosses: $(Fe_{0.88}Mg_{0.09}Mn_{0.03})CO_3$ at 1−3 GPa and 373 and 673 K, respectively, by H. Hu et al. (2022); black open squares: $MgCO_3$ at 700 and 1000 K at 3−6 GPa, respectively, by Mibe and Ono (2011). The error bar is shown as a vertical tick on the left bottom for clarity.

spin states of $FeCO_3$. The volume of $FeCO_3$ experiences a considerable decrease, up to 10%, as reported previously by synchrotron X-ray diffraction studies (Lavina et al., 2009, 2010; Liu et al., 2015). The density of charge carriers (n) exhibits a negative correlation with the unit cell volume V, following the relationship $n \propto 1/V$ (Yoshino, 2010). Consequently, the n values substantially increase with the ongoing volume collapse across the spin transition of iron. Moreover, the hopping distance between Fe^{2+} and Fe^{3+} decreases with increasing pressure due to the volume collapse, enhancing the mobility of small polarons (Yoshino, 2010). These factors collectively lead to the generation of dense charge carriers, improving the transport rate of electron-hole pairs and resulting in a significant increase in the EC of $FeCO_3$ at the spin crossover.

At pressures greater than ∼50 GPa, corresponding to the low-spin state of $FeCO_3$, the EC values slightly increase with increasing pressure. This could be attributed to a slight enhancement in the mobility of small polarons resulting from the volume compression of the unit cell as the pressure rises. Compared with the high-spin state, the decrease in the number of unpaired electrons in the low-spin state leads to a reduction in the number of small polarons (Ohta et al., 2010); however, the positive pressure effect outweighs the negative impact of unpaired electrons, resulting in a slight increase in the EC values of $FeCO_3$ in the low-spin state.

Remarkably, the EC values of $FeCO_3$, obtained in this study through the standard four-probe direct current techniques in DAC, are comparable to those of $(Fe_{0.88}Mg_{0.09}Mn_{0.03})CO_3$ measured at 1−3 GPa using a large volume multi-anvil apparatus (H. Hu et al., 2022) (Figure 2). Additionally, a representative EC measurement result at 50.8 GPa and 300 K is shown in Table S1 in Supporting Information S1. The measured EC values are relatively stable within 0.02 $\log_{10}\sigma$ (S/m) and consistent in different runs. These results demonstrate the repeatability and reliability of the high-pressure electrical measurements in the present work.

Furthermore, $Fe_{0.65}Mg_{0.35}CO_3$ exhibits a similar evolution of EC as $FeCO_3$ across the spin transition of iron (Figure S2 in Supporting Information S1). The substantial increase in the EC at ∼20 GPa is largely due to sample compaction and rapid changes in grain boundaries upon initial compression in DACs. The other substantial increase at ∼35 GPa is associated with the onset of the electronic spin-pairing transition of iron in $(Mg_{0.35}Fe_{0.65})CO_3$. Due to the lower iron content, the EC values of $Fe_{0.65}Mg_{0.35}CO_3$ are approximately 0.1–0.4 $\log_{10}$S/m (3%–9%) and 0.9–1.4 $\log_{10}$S/m (53%–94%) lower than those of $FeCO_3$ in the high-spin and low-spin states, respectively. It is noteworthy that the onset pressure of iron spin transition of $Fe_{0.65}Mg_{0.35}CO_3$ in this study is ∼8 GPa lower than our previous study (Liu et al., 2015). The lower onset spin pressure could be attributed to the existence of higher deviatoric stress in the sample chamber with the use of NaCl as a pressure-transmitting medium and/or the ruby calibrant located slightly further away from the $Fe_{0.65}Mg_{0.35}CO_3$ sample, leading to an underestimation of pressures in electrical measurements. After correction of the pressure shift, the EC values of $(Fe_{0.65}Mg_{0.35})CO_3$ are consistent with those extrapolated from the EC of $FeCO_3$ by multiplying a factor of 0.65 (Figure S2 in Supporting Information S1). Additionally, the EC values are increased by 1.7 orders of magnitude from the high-spin to low-spin states for $Fe_{0.65}Mg_{0.35}CO_3$, about 38% less than $FeCO_3$. This can be attributed to 35% Mg-substitution in (Mg, Fe)CO_3 solid solutions in the low-spin state, suggesting a roughly linear relationship between EC and iron content at the spin crossover.

3.2. Temperature Effect on the EC of (Mg, Fe)CO_3 at High Pressure

We further performed EC measurements on $FeCO_3$ at 10−60 GPa and 1500–2000 K to assess the effect of high temperature on the EC of (Mg, Fe)CO_3 (Figure 2). In the high-spin state, the EC of $FeCO_3$ is about −4.5 $\log_{10}$S/m at 300 K and ∼10−30 GPa, rising to +1.4 $\log_{10}$S/m at 1500 K in the same pressure range. This indicates a strong effect of high temperature on the EC of $FeCO_3$ by an increase of about 6 orders of magnitude throughout the deep-mantle *P-T*. Besides, at 3 GPa, the EC of $(Fe_{0.88}Mg_{0.09}Mn_{0.03})CO_3$ increases from −6.02 $\log_{10}$S/m at 373 K to −4.33 $\log_{10}$S/m at 673 K. Assuming a linear increase of EC with temperature, the EC of $(Fe_{0.88}Mg_{0.09}Mn_{0.03})CO_3$ would increase by about 7 orders of magnitude from 300 to 1500 K, which is comparable to the EC increase by about 6 orders of magnitude of $FeCO_3$ from this study. This effect is notably more pronounced in $MgCO_3$ (Mibe & Ono, 2011), where at 3−6 GPa, the EC of $MgCO_3$ increases by ∼3 orders of magnitude from 700 to 1000 K (Mibe & Ono, 2011). The EC of $MgCO_3$ might rise by ∼11 $\log_{10}$S/m from 300 to 1500 K at a given pressure. Unfortunately, at the higher temperature of 2000 K and 30−60 GPa, $FeCO_3$ partly decomposes and/or recrystallizes to $FeCO_3 + Fe_3O_4 \pm C$ mixtures, according to our Raman spectroscopy and XRD studies (Liu et al., 2015; Zhao et al., 2020), as well as previous XRD and XANES spectroscopy studies (Boulard et al., 2012; Cerantola et al., 2017, 2019) (Figures S3 and S4 in Supporting Information S1). When we analyzed Raman spectra of the recovered $FeCO_3$ sample (quenched at 58 GPa and 2000 K), a clear ν_1 mode of $FeCO_3$ and a possible high-pressure phase of Fe_3O_4 was recognized, indicating the partial decomposition and/or recrystallization of the initial $FeCO_3$ sample at 58 GPa and 2000 K (Figure S3a in Supporting Information S1) (Lin et al., 2014; Zhao et al., 2020). It was further observed that the Raman peak position of the ν_1 mode decreased at 45.4 GPa, and then abnormally increased at 31.5 GPa, confirming the spin transition of iron in $FeCO_3$ (Figure S3b in Supporting Information S1) (Zhao et al., 2020).

Moreover, we measured the EC of the quenched sample at 54 GPa and 300 K, and the EC value is located between the results at 300 and 2000 K (Figure 2). Particularly, the EC value of this quenched mixture $FeCO_3 + Fe_3O_4 \pm C$ from this study is comparable to the value of the mixture $FeCO_3 + Fe_3O_4 + C$ from the different method by H. Hu et al. (2022). These results confirm the mixture composition of $FeCO_3 + Fe_3O_4 \pm C$ and the high *P-T* phase diagram of $FeCO_3$. Meanwhile, due to the overlapping Raman signals with diamond anvils, we cannot clarify whether the existence of C in the mixture, thus using "$FeCO_3 + Fe_3O_4 \pm C$" to explain the recovered product. The EC values of the mixture $FeCO_3 + Fe_3O_4 \pm C$ are slightly greater than that of $FeCO_3$, increasing mildly with increasing pressure and reaching to +2.4 $\log_{10}$S/m at 58 GPa and 2000 K.

3.3. Comparison With the EC of the Major Lower-Mantle Minerals

The EC values of ferropericlase gradually increase by half an order of magnitude from −2.9 $\log_{10}$S/m at 15 GPa to −2.5 $\log_{10}$S/m at 50 GPa in the high-spin state, and then decrease by the same magnitude from −2.5 $\log_{10}$S/m at 50 to −2.8 $\log_{10}$S/m at 70 GPa, corresponding to its spin crossover (Lin et al., 2007; Yoshino et al., 2011) (Figure S5a in Supporting Information S1). The EC of bridgmanite also exhibits a comparable decrease from around −2.2 to −2.8 $\log_{10}$S/m at the spin crossover of 70–85 GPa (Ohta et al., 2010). In contrast, the EC of $FeCO_3$ increases remarkably by ∼3 orders of magnitude across the spin transition at ∼38−50 GPa, with respect to bridgmanite and ferropericlase. Despite sharing the same small polaron conduction mechanism at room temperature, the distinct electrical behaviors may result from significant differences in volume reduction and crystal structure (e.g., atomic arrangement and chemical bonding) across the spin transition of iron in mantle minerals (Lin et al., 2007; Yoshino, 2010; Yoshino et al., 2016) (More details can be referred to the Text S2 in Supporting Information S1).

At high *P-T* conditions of the lower mantle, the EC of (Mg, Fe)CO_3, ferropericlase and bridgmanite significantly increases at high temperatures, due to the pronounced enhancement of concentration and thermally activated mobility of charge carriers with rising temperature (Figure S5b in Supporting Information S1). Although the EC of (Mg, Fe)CO_3 is not well constrained at high pressure above 30 GPa and 1500 K, a first-order approximation of the effect of high temperature and iron content can be estimated from this study as reported in ferropericlase (Sinmyo et al., 2014; Yoshino et al., 2011) (Figure S5b in Supporting Information S1). Considering the average Fe/Mg molar ratio of ∼0.12 in Earth's mantle (McDonough & Sun, 1995), the chemical composition of candidate (Mg, Fe)CO_3 in the mantle is $(Mg_{0.85}Fe_{0.15})CO_3$. We extrapolated the EC of $(Mg_{0.85}Fe_{0.15})CO_3$ and $FeCO_3$ to high *P-T* conditions of the lower mantle, according to the EC results of $FeCO_3$ and $Fe_{0.65}Mg_{0.35}CO_3$ from this study as a similar interpolation successfully used to calculate the elasticity (e.g., sound velocity) of $(Mg_{0.9}Fe_{0.1})CO_3$ from $MgCO_3$ and $(Mg_{0.35}Fe_{0.65})CO_3$ (Liu et al., 2020).

Intriguingly, the EC of (Mg, Fe)CO_3 and $FeCO_3$ + Fe_3O_4 ± C mixtures may be enhanced by at least 6 $\log_{10}$S/m from room temperature to near adiabatic geotherm temperature conditions under deep mantle pressures. For ferropericlase, the EC increases by ∼4 $\log_{10}$S/m, ranging from −0.1 to +0.5 $\log_{10}$S/m under adiabatic geotherm conditions. Bridgmanite shows an increase of ∼3 $\log_{10}$S/m, ranging from 0.1 to 1.2 $\log_{10}$S/m under the same conditions (Sinmyo et al., 2014; Yoshino et al., 2011). Such large EC differences can be attributed to their crystal structures. (Mg, Fe)O_6 octahedra in (Mg, Fe)CO_3 is only corner-sharing and effectively isolated by CO_3^{2-} units, while (Mg, Fe)O_6 octahedra in ferropericlase and bridgmanite is closely packed via edge- or face-sharing (Hsu et al., 2021). Fe-Fe interactions are thus the weakest for (Mg, Fe)CO_3 among (Mg, Fe)CO_3, ferropericlase, and bridgmanite, resulting in the fastest mobility of small polarons with virtually unrestricted movement in (Mg, Fe)CO_3. This result suggests high temperature can significantly increase the EC of (Mg, Fe)CO_3 under lower-mantle conditions.

4. Geophysical Implications

Magnetotelluric data and geomagnetic depth sounding observations reported large discrepancies in local geomagnetic heterogeneities in the mid-lower mantle (Constable & Constable, 2004; Kuvshinov & Olsen, 2006; Kuvshinov et al., 2005; Tarits & Mandéa, 2010; Velímský, 2010). Those geomagnetic heterogeneities may be closely related to subducted slabs materials (Goes et al., 2017; Tarits & Mandéa, 2010). Notably, the EC values of major lower-mantle minerals (e.g., ferropericlase, bridgmanite, and davemaoite) exhibit mild changes at relevant depths (Lin et al., 2007; Ohta et al., 2007, 2010; Sinmyo et al., 2014; Yoshino et al., 2016). Consequently, the substantial increase in local geomagnetic anomalies points out the existence of high conductive materials in the region.

The EC evolution of (Mg, Fe)CO_3 solid solutions is strongly linked to the effects of high pressure, high temperature and iron content, resulting in their anomalous electrical behaviors at the spin crossover. This result sheds insights into their contributions on the local geomagnetic heterogeneities in the mid-lower mantle and subducted slabs, as well as on the mechanism driving Earth's deep carbon cycle. Particularly, the present study reveals that the EC values of (Mg, Fe)CO_3 and $FeCO_3$ + Fe_3O_4 ± C mixtures surpass major lower-mantle minerals by approximately 1–4 orders of magnitude at the depths of ∼800–2,000 km (Figure 3a). Although (Mg, Fe)CO_3-rich mineral is not a major constituent throughout the deep mantle, its impacts may still be significant. For example, even at very low-volume fractions (0.1 vol.%), carbon-bearing materials can still form interconnected networks at the grain boundaries of major mantle silicate minerals (Desmaele et al., 2019; Gaillard et al., 2008; Ono & Mibe, 2013; Yoshino et al., 2018). The relatively small amounts of carbonates (0.1 vol.%) have been proposed to elucidate high EC anomalies in the asthenosphere and shallow subduction zones (Desmaele et al., 2019; Gaillard et al., 2008; Ono & Mibe, 2013; Yoshino et al., 2018).

(Mg, Fe)CO_3-rich patches are probably subducted to lower-mantle depths along with subducted slabs and they may be accumulated locally and dispersed throughout the mantle through the deep carbon cycle and material exchange between subduction slabs and the surrounding mantle over geological time (Figure 3b and Text S3 in Supporting Information S1 for more details). The existence of (Mg, Fe)CO_3-rich patches likely lead to the formation of enhanced EC regions and thus local geomagnetic anomalies, compared to the surrounding mantle that are likely made of major constituent minerals (Cerantola et al., 2019; Li & Stackhouse, 2020; Lobanov et al., 2015). Considering the pyrolite compositional model, where bridgmanite, ferropericlase, and davemaoite constitute 78, 14, and 8 vol.%, respectively (Satta et al., 2021), it is estimated that 0.1 vol.% $(Mg_{0.85}Fe_{0.15})CO_3$ (8−21 vol.% $FeCO_3$) may cause a dramatic increase by 1.2 $\log_{10}$S/m at ∼1,300 km deep. In carbonated eclogite and peridotite lithologies, carbon is introduced into the deep mantle via subduction of carbonated oceanic crust containing about 5 wt.% CO_2 (Dasgupta & Hirschmann, 2006; Dasgupta et al., 2004; Sanchez-Valle et al., 2011). $(Mg_{0.85}Fe_{0.15})CO_3$ could be chemical composition of the major low-mantle carbonate due to its high stability even at the *P-T* conditions of the lower mantle geotherm (Binck et al., 2020; Isshiki et al., 2004). If half of the deep carbon transformed into $(Mg_{0.85}Fe_{0.15})CO_3$ (Shatskiy et al., 2023), there will be 5.8 vol.% and 7.2 vol.% $(Mg_{0.85}Fe_{0.15})CO_3$ in carbonated eclogite and peridotite lithologies, respectively. These values are much higher than the 0.1 vol.% fraction of $(Mg_{0.85}Fe_{0.15})CO_3$ to account for the geomagnetic observation anomalies at ∼1,300 km (Constable & Constable, 2004; Velímský, 2010). Besides, when half of the deep carbon is assumed to be transformed into $FeCO_3$, there will be 7.5 vol.% and 9.3 vol.% $FeCO_3$ in the carbonated eclogite and peridotite lithologies, respectively. These values are comparable to the lower bound of the fraction (i.e., ∼8.0 vol.%) of $FeCO_3$ to explain the geomagnetic observation anomalies. Given the EC of $FeCO_3$ + Fe_3O_4 ± C mixtures are comparable with the value

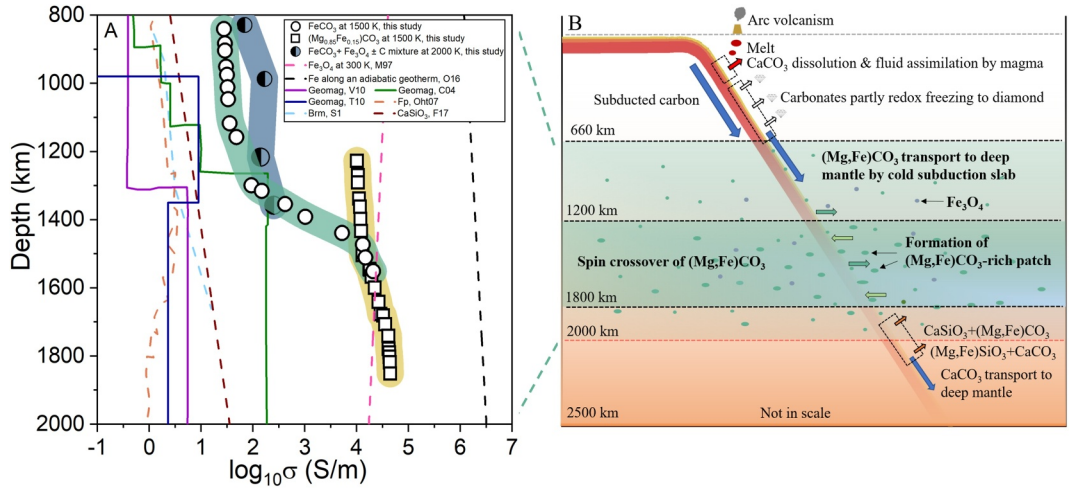

Figure 3. The electrical conductivity (EC) of (Mg, Fe)CO_3 and major minerals in the mantle along a subduction-related mantle geotherm (a) and a schematic illustration of carbonate fate in the oceanic crusts (orange) subducted to the lower mantle. Open black circles within the green shaded curve: $FeCO_3$ at 1500 K, this study; half-filled circles within the gray curve: $FeCO_3 + Fe_3O_4 \pm C$ at 2000 K, this study; open squares within the yellow curve: $(Mg_{0.85}Fe_{0.15})CO_3$ at 1500 K, this study; wine dashed curve: $CaSiO_3$ perovskite by Fei et al. (2017) (F17); orange dashed curve: ferropericlase (Fp) by Sinmyo et al. (2014) (S14) and Ohta et al. (2007) (O07); light blue dashed curve: bridgmanite (Brm) by Sinmyo et al. (2014) (S14); black pink curve: Fe_3O_4, Morris and Williams (1997) (M97); black dashed curve: Fe by Ohta et al. (2016) (O16); royal, purple, and olive solid curves: geomagnetic observations by Tarits and Mandéa (2010) (T10), Constable and Constable (2004) (C04), and Velímský (2010) (V10), respectively. The geotherm was taken from the literature (Fei et al., 2017; Katsura et al., 2010). During subduction, the majority of $CaCO_3$-rich carbonates could be dissolved and/or assimilated by magma at the depths of ~50–150 km (red arrow); the majority of (Mg, Fe)CO_3-rich carbonates may enter the deep mantle through subducted slabs, and part of (Mg, Fe)CO_3 carbonates may undergo redox freezing with metallic iron at ~200−700 km (white arrows); iron-partitioning into (Mg, Fe)CO_3 carbonates with respect to bridgmanite and the high-spin to low-spin transition of Fe^{2+}, and formation of (Mg, Fe)CO_3-rich and/or Fe_3O_4-rich domains/patches (green shaded region) at ~660−2,000 km; exchange reaction with lower-mantle silicates and transformation from (Mg, Fe)CO_3 to $CaCO_3$ at ~2,000 km (orange arrows). The green shaded zone at the depths of ~660–2,000 km corresponds to the region of the formation of high EC (Mg, Fe)CO_3-rich and $FeCO_3 + Fe_3O_4 \pm C$ mixtures domains/patches, which could contribute to the geomagnetic observation anomalies at ~1,300 km deep and local geomagnetic heterogeneities in the mid-lower mantle, as well as assist in identifying potential carbonate-rich regions in the Earth's deep interior. The spin crossover of (Mg, Fe)CO_3 occurs at the depths of 1,200–1,800 km. Furthermore, (Mg, Fe)CO_3 reacts with $CaSiO_3$ at 88 GPa and 1800 K, leading to the potential formation of (Mg, Fe)SiO_3 and $CaCO_3$ under deep lower-mantle conditions (Lv et al., 2021). Ultimately, $CaCO_3$ may become the main carbonate at the depths of 2,000–2,900 km (panel (b)).

of $FeCO_3$ and possible coexisted with each other in the lower mantle. Therefore, the high EC of (Mg, Fe)CO_3-rich and $FeCO_3 + Fe_3O_4 \pm C$ mixtures patches can contribute, albeit locally, to the emerging of geomagnetic anomalies at ~1,300 km as well as local geomagnetic heterogeneities in the mid-mantle.

Interestingly, the elastic properties (e.g., velocity, anisotropy, and bulk modulus) of (Mg, Fe)CO_3 solid solutions also behave anomalously across the iron spin transition, which could have a significant influence on the seismic observations in the Earth's lower mantle (Fu et al., 2017; Liu et al., 2020; Marcondes et al., 2016; Stekiel et al., 2017). Similarly, the electrical and thermal conductivity of (Mg, Fe)CO_3 changes dramatically across the iron spin transition (Chao & Hsieh, 2019). Those dramatic changes may induce greater heat flux, higher temperature and iron content than the surrounding subducted slabs and pyrolytic mantle minerals, likely further causing local thermochemical conductivity and geomagnetic anomalies and altering the distribution fields of these minerals (Chao & Hsieh, 2019). This may also impact the fate of carbonates in the global carbon cycle. Therefore, these anomalous behaviors of (Mg, Fe)CO_3 at the spin crossover improve our understanding of global seismic observations and thermochemical anomalies in the Earth's lower mantle and can assist in identifying potential carbon-rich regions in the Earth's interior (Fu et al., 2017; Li & Stackhouse, 2020; Liu et al., 2015; Yang et al., 2014). Compared to those of the major minerals of the lower mantle, the high EC and low velocity of Fe_3O_4-rich patches may potentially contribute to the local geomagnetic and/or seismic heterogeneities in the mid-lower mantle (Lin et al., 2014; Morris & Williams, 1997).

Data Availability Statement

Electrical conductivity data of (Mg, Fe)CO_3 and $FeCO_3$ + Fe_3O_4 ± C mixtures in Figures 1–3 and Table S1 in Supporting Information S1 are available at Zhao, Liu, et al. (2024).

Acknowledgments
We thank Zhu Mao, Xueyan Du, and Wenge Yang for constructive discussion and technical assistance. This work is supported by the National Key Research and Development Program of China (2023YFF0804100, 2019YFA0708502). C. Zhao acknowledges support from the National Natural Science Foundation of China (42104101). J. Liu acknowledges support from the National Natural Science Foundation of China (42072052) and the Natural Science Foundation of Hebei (D2024203001, 2023HBQZYCSB008). M. Hou acknowledges support from the Natural Science Foundation of China (42394114, 42394112). Some experiments are supported by the Synergic Extreme Condition User Facility (SECUF) and BL15U1 at the Shanghai Synchrotron Radiation Facility (SSRF proposal#2022-SSRF-PT-021393).

References

Akahama, Y., & Kawamura, H. (2010). Pressure calibration of diamond anvil Raman gauge to 410 GPa. *Journal of Physics: Conference Series*, *215*, 012195. https://doi.org/10.1088/1742-6596/215/1/012195

Behn, M. D., Kelemen, P. B., Hirth, G., Hacker, B. R., & Massonne, H. J. (2011). Diapirs as the source of the sediment signature in arc lavas. *Nature Geoscience*, *4*(9), 641–646. https://doi.org/10.1038/ngeo1214

Binck, J., Bayarjargal, L., Lobanov, S. S., Morgenroth, W., Luchitskaia, R., Pickard, C. J., et al. (2020). Phase stabilities of $MgCO_3$ and $MgCO_3$-II studied by Raman spectroscopy, X-ray diffraction, and density functional theory calculations. *Physical Review Materials*, *4*(5), 055001. https://doi.org/10.1103/physrevmaterials.4.055001

Boulard, E., Menguy, N., Auzende, A. L., Benzerara, K., Bureau, H., Antonangeli, D., et al. (2012). Experimental investigation of the stability of Fe-rich carbonates in the lower mantle. *Journal of Geophysical Research*, *117*(B2), B02208. https://doi.org/10.1029/2011jb008733

Brenker, F. E., Vollmer, C., Vincze, L., Vekemans, B., Szymanski, A., Janssens, K., et al. (2007). Carbonates from the lower part of transition zone or even the lower mantle. *Earth and Planetary Science Letters*, *260*(1–2), 1–9. https://doi.org/10.1016/j.epsl.2007.02.038

Cerantola, V., Bykova, E., Kupenko, I., Merlini, M., Ismailova, L., McCammon, C., et al. (2017). Stability of iron-bearing carbonates in the deep Earth's interior. *Nature Communications*, *8*(1), 15960. https://doi.org/10.1038/ncomms15960

Cerantola, V., McCammon, C., Kupenko, I., Kantor, I., Marini, C., Wilke, M., et al. (2015). High-pressure spectroscopic study of siderite ($FeCO_3$) with a focus on spin crossover. *American Mineralogist*, *100*(11–12), 2670–2681. https://doi.org/10.2138/am-2015-5319

Cerantola, V., Wilke, M., Kantor, I., Ismailova, L., Kupenko, I., McCammon, C., et al. (2019). Experimental investigation of $FeCO_3$ (siderite) stability in Earth's lower mantle using XANES spectroscopy. *American Mineralogist*, *104*(8), 1083–1091. https://doi.org/10.2138/am-2019-6428

Chao, K. H., & Hsieh, W. P. (2019). Thermal conductivity anomaly in $(Fe_{0.78}Mg_{0.22})CO_3$ siderite across spin transition of iron. *Journal of Geophysical Research: Solid Earth*, *124*(2), 1388–1396. https://doi.org/10.1029/2018jb017003

Constable, S., & Constable, C. (2004). Observing geomagnetic induction in magnetic satellite measurements and associated implications for mantle conductivity. *Geochemistry, Geophysics, Geosystems*, *5*(1), Q01006. https://doi.org/10.1029/2003gc000634

Dasgupta, R., & Hirschmann, M. M. (2006). Melting in the Earth's deep upper mantle caused by carbon dioxide. *Nature*, *440*(7084), 659–662. https://doi.org/10.1038/nature04612

Dasgupta, R., Hirschmann, M. M., & Withers, A. C. (2004). Deep global cycling of carbon constrained by the solidus of anhydrous, carbonated eclogite under upper mantle conditions. *Earth and Planetary Science Letters*, *227*(1–2), 73–85. https://doi.org/10.1016/j.epsl.2004.08.004

Desmaele, E., Sator, N., Vuilleumier, R., & Guillot, B. (2019). Atomistic simulations of molten carbonates: Thermodynamic and transport properties of the Li_2CO_3-Na_2CO_3-K_2CO_3 system. *Journal of Chemical Physics*, *150*(9), 094504. https://doi.org/10.1063/1.5082731

Dobson, D. P., & Brodholt, J. P. (2000). The electrical conductivity of the lower mantle phase magnesiowüstite at high temperatures and pressures. *Journal of Geophysical Research*, *105*(B1), 531–538. https://doi.org/10.1029/1999jb900242

Farsang, S., Louvel, M., Zhao, C., Mezouar, M., Rosa, A. D., Widmer, R. N., et al. (2021). Deep carbon cycle constrained by carbonate solubility. *Nature Communications*, *12*(1), 4311. https://doi.org/10.1038/s41467-021-24533-7

Fei, H., Huang, R., & Yang, X. (2017). $CaSiO_3$ perovskite may cause electrical conductivity jump in the topmost lower mantle. *Geophysical Research Letters*, *44*(20), 10226. https://doi.org/10.1002/2017gl075070

Foley, S. F., & Fischer, T. P. (2017). An essential role for continental rifts and lithosphere in the deep carbon cycle. *Nature Geoscience*, *10*(12), 897–902. https://doi.org/10.1038/s41561-017-0002-7

Fu, S., Yang, J., & Lin, J. F. (2017). Abnormal elasticity of single-crystal magnesiosiderite across the spin transition in Earth's lower mantle. *Physical Review Letters*, *118*(3), 036402. https://doi.org/10.1103/physrevlett.118.036402

Gaillard, F., Malki, M., Iacono-Marziano, G., Pichavant, M., & Scaillet, B. (2008). Carbonatite melts and electrical conductivity in the asthenosphere. *Science*, *322*(5906), 1363–1365. https://doi.org/10.1126/science.1164446

Goes, S., Agrusta, R., van Hunen, J., & Garel, F. (2017). Subduction-transition zone interaction: A review. *Geosphere*, *13*(3), 644–664. https://doi.org/10.1130/ges01476.1

Hazen, R. M., & Schiffries, C. M. (2013). Why deep carbon? *Reviews in Mineralogy and Geochemistry*, *75*(1), 1–6. https://doi.org/10.2138/rmg.2013.75.1

Hou, M., He, Y., Jang, B. G., Sun, S., Zhuang, Y., Deng, L., et al. (2021). Superionic iron oxide–hydroxide in Earth's deep mantle. *Nature Geoscience*, *14*(3), 174–178. https://doi.org/10.1038/s41561-021-00696-2

Hsu, H., Crisostomo, C. P., Wang, W., & Wu, Z. (2021). Anomalous thermal properties and spin crossover of ferromagnesite (Mg, Fe)CO_3. *Physical Review B*, *103*(5), 054401. https://doi.org/10.1103/physrevb.103.054401

Hu, H., Jing, C., Dai, L., Yin, C., & Chen, D. (2022). Electrical conductivity of siderite and its implication for high conductivity anomaly in the slab-mantle wedge interface. *Frontiers in Earth Science*, *10*, 985740. https://doi.org/10.3389/feart.2022.985740

Hu, J., Xu, L. X., Liu, J., & Yue, D. H. (2023). Effects of spin transition and cation substitution on the optical properties and iron partitioning in carbonate minerals. *Acta Geologica Sinica*, *97*(1), 350–357. https://doi.org/10.1111/1755-6724.15042

Isshiki, M., Irifune, T., Hirose, K., Ono, S., Ohishi, Y., Watanuki, T., et al. (2004). Stability of magnesite and its high-pressure form in the lowermost mantle. *Nature*, *427*(6969), 60–63. https://doi.org/10.1038/nature02181

Katsura, T., Yoneda, A., Yamazaki, D., Yoshino, T., & Ito, E. (2010). Adiabatic temperature profile in the mantle. *Physics of the Earth and Planetary Interiors*, *183*(1–2), 212–218. https://doi.org/10.1016/j.pepi.2010.07.001

Kelemen, P. B., & Manning, C. E. (2015). Reevaluating carbon fluxes in subduction zones, what goes down, mostly comes up. *Proceedings of the National Academy of Sciences of the United States of America*, *112*(30), E3997–E4006. https://doi.org/10.1073/pnas.1507889112

Kuvshinov, A., & Olsen, N. (2006). A global model of mantle conductivity derived from 5 years of CHAMP, Ørsted, and SAC-C magnetic data. *Geophysical Research Letters*, *33*(18), L18301. https://doi.org/10.1029/2006gl027083

Kuvshinov, A., Utada, H., Avdeev, D., & Koyama, T. (2005). 3-D modelling and analysis of Dst C-responses in the North Pacific Ocean region, revisited. *Geophysical Journal International*, *160*(2), 505–526. https://doi.org/10.1111/j.1365-246x.2005.02477.x

Lavina, B., Dera, P., Downs, R. T., Prakapenka, V., Rivers, M., Sutton, S., & Nicol, M. (2009). Siderite at lower mantle conditions and the effects of the pressure-induced spin-pairing transition. *Geophysical Research Letters*, *36*(23), L23306. https://doi.org/10.1029/2009gl039652

Lavina, B., Dera, P., Downs, R. T., Yang, W. G., Sinogeikin, S., Meng, Y., et al. (2010). Structure of siderite $FeCO_3$ to 56 GPa and hysteresis of its spin-pairing transition. *Physical Review B*, *82*(6), 064110. https://doi.org/10.1103/physrevb.82.064110

Lee, H., Muirhead, J. D., Fischer, T. P., Ebinger, C. J., Kattenhorn, S. A., Sharp, Z. D., & Kianji, G. (2016). Massive and prolonged deep carbon emissions associated with continental rifting. *Nature Geoscience*, *9*(2), 145–149. https://doi.org/10.1038/ngeo2622

Li, Z., & Stackhouse, S. (2020). Iron-rich carbonates stabilized by magnetic entropy at lower mantle conditions. *Earth and Planetary Science Letters*, *531*, 115959. https://doi.org/10.1016/j.epsl.2019.115959

Lin, J. F., Speziale, S., Mao, Z., & Marquardt, H. (2013). Effects of the electronic spin transitions of iron in lower mantle minerals: Implications for deep mantle geophysics and geochemistry. *Reviews of Geophysics*, *51*(2), 244–275. https://doi.org/10.1002/rog.20010

Lin, J. F., Weir, S. T., Jackson, D. D., Evans, W. J., Vohra, Y. K., Qiu, W., & Yoo, C.-S. (2007). Electrical conductivity of the lower-mantle ferropericlase across the electronic spin transition. *Geophysical Research Letters*, *34*(16), L16305. https://doi.org/10.1029/2007gl030523

Lin, J. F., Wu, J., Zhu, J., Mao, Z., Said, A. H., Leu, B. M., et al. (2014). Abnormal elastic and vibrational behaviors of magnetite at high pressures. *Scientific Reports*, *4*(1), 6282. https://doi.org/10.1038/srep06282

Liu, J., Dorfman, S. M., Zhu, F., Li, J., Wang, Y., Zhang, D., et al. (2018). Valence and spin states of iron are invisible in Earth's lower mantle. *Nature Communications*, *9*(1), 1284. https://doi.org/10.1038/s41467-018-03671-5

Liu, J., Lin, J. F., Mao, Z., & Prakapenka, V. B. (2014). Thermal equation of state and spin transition of magnesiosiderite at high pressure and temperature. *American Mineralogist*, *99*(1), 84–93. https://doi.org/10.2138/am.2014.4553

Liu, J., Lin, J. F., & Prakapenka, V. B. (2015). High-pressure orthorhombic ferromagnesite as a potential deep-mantle carbon carrier. *Scientific Reports*, *5*(1), 7640. https://doi.org/10.1038/srep07640

Liu, J. C., Fu, S. Y., & Lin, J. F. (2020). Spin transition of iron in deep-mantle ferromagnesite. In *Carbon in Earth's Interior*, *Geophysical Monograph* (Vol. 249).

Lobanov, S. S., Goncharov, A. F., & Litasov, K. D. (2015). Optical properties of siderite ($FeCO_3$) across the spin transition: Crossover to iron-rich carbonates in the lower mantle. *American Mineralogist*, *100*(5–6), 1059–1064. https://doi.org/10.2138/am-2015-5053

Lv, M., Dorfman, S. M., Badro, J., Borensztajn, S., Greenberg, E., & Prakapenka, V. B. (2021). Reversal of carbonate-silicate cation exchange in cold slabs in Earth's lower mantle. *Nature Communications*, *12*(1), 1712. https://doi.org/10.1038/s41467-021-21761-9

Maeda, F., Ohtani, E., Kamada, S., Sakamaki, T., Hirao, N., & Ohishi, Y. (2017). Diamond formation in the deep lower mantle: A high-pressure reaction of $MgCO_3$ and SiO_2. *Scientific Reports*, *7*(1), 40602. https://doi.org/10.1038/srep40602

Mao, H., Xu, J. A., & Bell, P. (1986). Calibration of the ruby pressure gauge to 800 kbar under quasi-hydrostatic conditions. *Journal of Geophysical Research*, *91*(B5), 4673–4676. https://doi.org/10.1029/jb091ib05p04673

Mao, Z., Lin, J. F., Liu, J., & Prakapenka, V. B. (2011). Thermal equation of state of lower-mantle ferropericlase across the spin crossover. *Geophysical Research Letters*, *38*(23), L23308. https://doi.org/10.1029/2011gl049915

Mao, Z., Lin, J. F., Yang, J., Inoue, T., & Prakapenka, V. B. (2015). Effects of the Fe^{3+} spin transition on the equation of state of bridgmanite. *Geophysical Research Letters*, *42*(11), 4335–4342. https://doi.org/10.1002/2015gl064400

Marcondes, M. L., Justo, J. F., & Assali, L. V. C. (2016). Carbonates at high pressures: Possible carriers for deep carbon reservoirs in the Earth's lower mantle. *Physical Review B*, *94*(10), 104112. https://doi.org/10.1103/physrevb.94.104112

Mattila, A., Pylkkänen, T., Rueff, J. P., Huotari, S., Vankó, G., Hanfland, M., et al. (2007). Pressure induced magnetic transition in siderite $FeCO_3$ studied by X-ray emission spectroscopy. *Journal of Physics: Condensed Matter*, *19*(38), 386206. https://doi.org/10.1088/0953-8984/19/38/386206

McDonough, W. F., & Sun, S. S. (1995). The composition of the Earth. *Chemical Geology*, *120*(3–4), 223–253. https://doi.org/10.1016/0009-2541(94)00140-4

Mibe, K., & Ono, S. (2011). Electrical conductivity of $MgCO_3$ at high pressures and high temperatures. *Physica B: Condensed Matter*, *406*(10), 2018–2020. https://doi.org/10.1016/j.physb.2011.03.009

Morris, E. R., & Williams, Q. (1997). Electrical resistivity of Fe_3O_4 to 48 GPa: Compression-induced changes in electron hopping at mantle pressures. *Journal of Geophysical Research*, *102*(B8), 18139–18148. https://doi.org/10.1029/97jb00024

Ohta, K., Hirose, K., Onoda, S., & Shimizu, K. (2007). The effect of iron spin transition on electrical conductivity of (Mg, Fe)O magnesiowustite. *Proceedings of the Japan Academay Series B Physical and Biological Sciences*, *83*(3), 97–100. https://doi.org/10.2183/pjab.83.97

Ohta, K., Hirose, K., Shimizu, K., Sata, N., & Ohishi, Y. (2010). The electrical resistance measurements of (Mg, Fe)SiO_3 perovskite at high pressures and implications for electronic spin transition of iron. *Physics of the Earth and Planetary Interiors*, *180*(3–4), 154–158. https://doi.org/10.1016/j.pepi.2009.11.002

Ohta, K., Kuwayama, Y., Hirose, K., Shimizu, K., & Ohishi, Y. (2016). Experimental determination of the electrical resistivity of iron at Earth's core conditions. *Nature*, *534*(7605), 95–98. https://doi.org/10.1038/nature17957

Ono, S., & Mibe, K. (2013). Electrical conductivity of aragonite in the subducted slab. *European Journal of Mineralogy*, *25*(1), 11–15. https://doi.org/10.1127/0935-1221/2013/0025-2254

Pan, D., Spanu, L., Harrison, B., Sverjensky, D. A., & Galli, G. (2013). Dielectric properties of water under extreme conditions and transport of carbonates in the deep Earth. *Proceedings of the National Academy of Sciences*, *110*(17), 6646–6650. https://doi.org/10.1073/pnas.1221581110

Papathanassiou, A. N. (1998). Effect of hydrostatic pressure on the electrical conductance of polycrystalline magnesite ($MgCO_3$). *Physical Review B*, *58*(8), 4432–4437. https://doi.org/10.1103/physrevb.58.4432

Plank, T., & Manning, C. E. (2019). Subducting carbon. *Nature*, *574*(7778), 343–352. https://doi.org/10.1038/s41586-019-1643-z

Poli, S. (2015). Carbon mobilized at shallow depths in subduction zones by carbonatitic liquids. *Nature Geoscience*, *8*(8), 633–636. https://doi.org/10.1038/ngeo2464

Prakash, A., Holyoke, III, C. W., Kelemen, P. B., Kirby, S. H., Kronenberg, A. K., & Lamb, W. M. (2023). Carbonates and intermediate-depth seismicity: Stable and unstable shear in altered subducting plates and overlying mantle. *Proceedings of the National Academy of Sciences of the United States of America*, *120*(21), e2219076120. https://doi.org/10.1073/pnas.2219076120

Sanchez-Valle, C., Ghosh, S., & Rosa, A. D. (2011). Sound velocities of ferromagnesian carbonates and the seismic detection of carbonates in eclogites and the mantle. *Geophysical Research Letters*, *38*(24), L24315. https://doi.org/10.1029/2011gl049981

Satta, N., Criniti, G., Kurnosov, A., Boffa Ballaran, T., Ishii, T., & Marquardt, H. (2021). High-pressure elasticity of δ-(Al, Fe)OOH single crystals and seismic detectability of hydrous MORB in the shallow lower mantle. *Geophysical Research Letters*, *48*(23), e2021GL094185. https://doi.org/10.1029/2021gl094185

Shatskiy, A., Arefiev, A. V., & Litasov, K. D. (2023). Change in carbonate budget and composition during subduction below metal saturation boundary. *Geoscience Frontiers*, *14*(1), 101463. https://doi.org/10.1016/j.gsf.2022.101463

Shcheka, S. S., Wiedenbeck, M., Frost, D. J., & Keppler, H. (2006). Carbon solubility in mantle minerals. *Earth and Planetary Science Letters*, *245*(3–4), 730–742. https://doi.org/10.1016/j.epsl.2006.03.036

Shen, G., Rivers, M. L., Wang, Y., & Sutton, S. R. (2001). Laser heated diamond cell system at the Advanced Photon Source for in situ X-ray measurements at high pressure and temperature. *Review of Scientific Instruments*, *72*(2), 1273–1282. https://doi.org/10.1063/1.1343867

Sinmyo, R., Pesce, G., Greenberg, E., McCammon, C., & Dubrovinsky, L. (2014). Lower mantle electrical conductivity based on measurements of Al, Fe-bearing perovskite under lower mantle conditions. *Earth and Planetary Science Letters*, *393*, 165–172. https://doi.org/10.1016/j.epsl.2014.02.049

Stekiel, M., Nguyen-Thanh, T., Chariton, S., McCammon, C., Bosak, A., Morgenroth, W., et al. (2017). High pressure elasticity of $FeCO_3$-$MgCO_3$ carbonates. *Physics of the Earth and Planetary Interiors*, *271*, 57–63. https://doi.org/10.1016/j.pepi.2017.08.004

Sun, Y., Hier-Majumder, S., Xu, Y., & Walter, M. (2020). Stability and migration of slab-derived carbonate-rich melts above the transition zone. *Earth and Planetary Science Letters*, *531*, 116000. https://doi.org/10.1016/j.epsl.2019.116000

Tarits, P., & Mandéa, M. (2010). The heterogeneous electrical conductivity structure of the lower mantle. *Physics of the Earth and Planetary Interiors*, *183*(1–2), 115–125. https://doi.org/10.1016/j.pepi.2010.08.002

Thomson, A. R., Walter, M. J., Kohn, S. C., & Brooker, R. A. (2016). Slab melting as a barrier to deep carbon subduction. *Nature*, *529*(7584), 76–79. https://doi.org/10.1038/nature16174

Timmerman, S., Spivak, A. V., & Jones, A. P. (2021). Carbonatitic melts and their role in diamond formation in the deep Earth. *Elements*, *17*(5), 321–326. https://doi.org/10.2138/gselements.17.5.321

Velímský, J. (2010). Electrical conductivity in the lower mantle: Constraints from CHAMP satellite data by time-domain EM induction modelling. *Physics of the Earth and Planetary Interiors*, *180*(3–4), 111–117. https://doi.org/10.1016/j.pepi.2010.02.007

Yang, J., Mao, Z., Lin, J.-F., & Prakapenka, V. B. (2014). Single-crystal elasticity of the deep-mantle magnesite at high pressure and temperature. *Earth and Planetary Science Letters*, *392*, 292–299. https://doi.org/10.1016/j.epsl.2014.01.027

Yoshino, T. (2010). Laboratory electrical conductivity measurement of mantle minerals. *Surveys in Geophysics*, *31*(2), 163–206. https://doi.org/10.1007/s10712-009-9084-0

Yoshino, T., Gruber, B., & Reinier, C. (2018). Effects of pressure and water on electrical conductivity of carbonate melt with implications for conductivity anomaly in continental mantle lithosphere. *Physics of the Earth and Planetary Interiors*, *281*, 8–16. https://doi.org/10.1016/j.pepi.2018.05.003

Yoshino, T., Ito, E., Katsura, T., Yamazaki, D., Shan, S., Guo, X., et al. (2011). Effect of iron content on electrical conductivity of ferropericlase with implications for the spin transition pressure. *Journal of Geophysical Research*, *116*(B4), B04202. https://doi.org/10.1029/2010jb007801

Yoshino, T., Kamada, S., Zhao, C., Ohtani, E., & Hirao, N. (2016). Electrical conductivity model of Al-bearing bridgmanite with implications for the electrical structure of the Earth's lower mantle. *Earth and Planetary Science Letters*, *434*, 208–219. https://doi.org/10.1016/j.epsl.2015.11.032

Zhang, X. Y., Chen, L. H., Wang, X. J., Hanyu, T., Hofmann, A. W., Komiya, T., et al. (2022). Zinc isotopic evidence for recycled carbonate in the deep mantle. *Nature Communications*, *13*(1), 6085. https://doi.org/10.1038/s41467-022-33789-6

Zhao, C., Liu, J., Xu, L., Hou, M., Zhuang, Y., & Zhu, J. (2024). (Mg, Fe)CO_3_Electrical conductivity_dataset.xlsx [Dataset]. *figshare*. https://doi.org/10.6084/m9.figshare.25217873.v4

Zhao, C., Mao, Z., Anna, S., Zhang, X., Yu, Y., Li, L., et al. (2024). Anomalous vibrational properties and spin phase diagrams of (Mg, Fe)CO_3 under extreme conditions. *Physical Review B*, *109*(22), 224110. https://doi.org/10.1103/physrevb.109.224110

Zhao, C., Xu, L., Gui, W., & Liu, J. (2020). Phase stability and vibrational properties of iron-bearing carbonates at high pressure. *Minerals*, *10*(12), 1142. https://doi.org/10.3390/min10121142

References From the Supporting Information

Bower, D. J., Gurnis, M., & Seton, M. (2013). Lower mantle structure from paleogeographically constrained dynamic Earth models. *Geochemistry, Geophysics, Geosystems*, *14*(1), 44–63. https://doi.org/10.1029/2012gc004267

Clift, P. D. (2017). A revised budget for Cenozoic sedimentary carbon subduction. *Reviews of Geophysics*, *55*(1), 97–125. https://doi.org/10.1002/2016rg000531

Fei, Y., Zhang, L., Corgne, A., Watson, H., Ricolleau, A., Meng, Y., & Prakapenka, V. (2007). Spin transition and equations of state of (Mg, Fe)O solid solutions. *Geophysical Research Letters*, *34*(17), L17307. https://doi.org/10.1029/2007gl030712

Hammouda, T., Manthilake, G., Goncalves, P., Chantel, J., Guignard, J., Crichton, W., & Gaillard, F. (2021). Is there a global carbonate layer in the oceanic mantle? *Geophysical Research Letters*, *48*(2), e2020GL089752. https://doi.org/10.1029/2020gl089752

Kaminsky, F. V. (2017). *The Earth's lower mantle composition and structure*. Springer.

Kang, N., Schmidt, M. W., Poli, S., Franzolin, E., & Connolly, J. A. D. (2015). Melting of siderite to 20 GPa and thermodynamic properties of $FeCO_3$-melt. *Chemical Geology*, *400*, 34–43. https://doi.org/10.1016/j.chemgeo.2015.02.005

Komabayashi, T., Omori, S., & Maruyama, S. (2004). Petrogenetic grid in the system MgO-SiO_2-H_2O up to 30 GPa, 1600°C: Applications to hydrous peridotite subducting into the Earth's deep interior. *Journal of Geophysical Research*, *109*(B3), B03206. https://doi.org/10.1029/2003jb002651

Li, K., Li, L., Pearson, D. G., & Stachel, T. (2019). Diamond isotope compositions indicate altered igneous oceanic crust dominates deep carbon recycling. *Earth and Planetary Science Letters*, *516*, 190–201. https://doi.org/10.1016/j.epsl.2019.03.041

Lin, J. F., Liu, J., Jacobs, C., & Prakapenka, V. B. (2012). Vibrational and elastic properties of ferromagnesite across the electronic spin-pairing transition of iron. *American Mineralogist*, *97*(4), 583–591. https://doi.org/10.2138/am.2012.3961

Lobanov, S. S., & Goncharov, A. F. (2020). Pressure-induced sp^2-sp^3 transitions in carbon-bearing phases. *Carbon in Earth's Interior*, 1–9.

Marquardt, H., & Thomson, A. R. (2020). Experimental elasticity of Earth's deep mantle. *Nature Reviews Earth & Environment*, *1*(9), 455–469. https://doi.org/10.1038/s43017-020-0077-3

Shim, S. H., Grocholski, B., Ye, Y., Alp, E. E., Xu, S., Morgan, D., et al. (2017). Stability of ferrous-iron-rich bridgmanite under reducing midmantle conditions. *Proceedings of the National Academy of Sciences*, *114*(25), 6468–6473. https://doi.org/10.1073/pnas.1614036114

Sun, W. D., Hawkesworth, C. J., Yao, C., Zhang, C. C., Huang, R. F., Liu, X., et al. (2018). Carbonated mantle domains at the base of the Earth's transition zone. *Chemical Geology*, *478*, 69–75. https://doi.org/10.1016/j.chemgeo.2017.08.001

Tackley, P. J. (2011). Living dead slabs in 3-D: The dynamics of compositionally-stratified slabs entering a "slab graveyard" above the core-mantle boundary. *Physics of the Earth and Planetary Interiors*, *188*(3–4), 150–162. https://doi.org/10.1016/j.pepi.2011.04.013

Tao, R., Fei, Y., & Zhang, L. (2013). Experimental determination of siderite stability at high pressure. *American Mineralogist*, *98*(8–9), 1565–1572. https://doi.org/10.2138/am.2013.4351

van der Meer, D. G., Spakman, W., van Hinsbergen, D. J. J., Amaru, M. L., & Torsvik, T. H. (2009). Towards absolute plate motions constrained by lower-mantle slab remnants. *Nature Geoscience*, *3*(1), 36–40. https://doi.org/10.1038/ngeo708

Wang, W., Xu, Y., Sun, D., Ni, S., Wentzcovitch, R., & Wu, Z. (2020). Velocity and density characteristics of subducted oceanic crust and the origin of lower-mantle heterogeneities. *Nature Communications*, *11*(1), 64. https://doi.org/10.1038/s41467-019-13720-2